Microfluidics and Nanofluidics (2024) 28:5
https://doi.org/10.1007/s10404-023-02700-0

RESEARCH

Experimental investigation of microparticle focusing in SiO_2 nanofluids inside curvilinear microchannels

Arsalan Nikdoost[1] · Pouya Rezai[1]

Received: 1 October 2023 / Accepted: 13 November 2023 / Published online: 20 December 2023

Abstract
Curvilinear microchannels have enabled high throughput sized-based separation and manipulation of microparticles. Real life applications usually deal with fluid's non-Newtonian behavior, where particles dynamics are altered compared to Newtonian mediums. Despite multiple reports on particle manipulation in shear-thinning fluids, no fundamental experimental investigation has been reported on microparticle focusing behavior inside shear-thickening fluids such as metallic oxide nanofluids in water (e.g., SiO_2-water). These nanofluids pose unique thermal characteristics and exhibit a drastic increase in viscosity as the shear rate rises in the microchannel. Here, we investigate the particle focusing behavior of co-flows of SiO_2 nanofluids inside curved microchannels with various channel widths and radii of curvature. We also report on the effect of nanofluid concentration, fluid axial velocity, and the particle size on particle migration. We observed a behavioral change in particle migration in SiO_2 nanofluids, where the shear-dependent effect could enhance the particle focusing at lower flow rates. Moreover, the dominance of Dean drag at higher axial velocities would dominate the particle migration and transfer them towards two focusing peaks close to the sidewalls. A thorough investigation of particle behavior in nanofluids inside curved microchannels could enable future applications in heat exchangers, solar energy collectors, and nanoplastic detection.

Keywords Microfluidics · Particle focusing · Nanofluids · Shear thickening · Particle sorting

1 Introduction

Separation, detection, and enrichment of target cells and microparticles are vital steps in many applications such as medicine, food and environmental monitoring, and microparticle coating (Tsai et al. 2011; Hur et al. 2012). Microfluidic platforms facilitate the accurate sample preparation at the point of need by integration of detection and analysis processes (Lee et al. 2015; Jiang et al. 2016). Microfluidic methods for particle and fluid manipulation are divided into active and passive techniques. Active methods are usually tunable in real time but require an external source of energy, which adds to the complexity and cost (Sivaramakrishnan et al. 2020). Common active methods such as acoustophoresis (Hawkes et al. 2004; Laurell et al. 2007), dielectrophoresis (Tornay et al. 2008; Li et al. 2014), and magnetophoresis (Peyman et al. 2009; Vojtíšek et al. 2010) are mainly associated with low working throughput and complex fabrication process or limited to magnetic and magnetically susceptible particles. Passive techniques, on the other hand, depend on the channel geometry and enable a precise control over the particle and fluid behavior solely through the manipulation of the flow induced forces such as inertial, drag, and elastic forces. Passive microfluidic techniques are robust, very simple to operate and work at high flow rates (Zhang et al. 2016).

Inside an inertial medium, microparticles with a blockage ratio of $\beta > 0.07$ are under the dominant effect of shear-induced and wall-induced lift forces (Segré and Silberberg 1961). The blockage ratio ($\beta = a/D_h$) (Di Carlo 2009) represents the ratio of particle diameter (a) with respect to the channel hydraulic diameter (D_h). These dominant inertial lift forces depend on the particle position in the microchannel and the flow Reynolds number ($\mathrm{Re} = \rho V D_h/\mu$) (Zhou and Papautsky 2013; Martel and Toner 2014). Here, fluid density and viscosity are denoted by ρ and μ, respectively; and V indicates the fluid velocity in the axial channel direction (V_x) or the lateral direction (V_L, i.e., secondary Dean flows in curvilinear microchannels).

✉ Pouya Rezai
prezai@yorku.ca

[1] Department of Mechanical Engineering, York University, BRG 433B, 4700 Keele St, Toronto, ON M3J 1P3, Canada

Inertial lift forces in straight microchannels could focus the microparticles on two or four equilibrium positions in microchannels with rectangular and square cross sections, respectively (Mach and di Carlo 2010; Gossett et al. 2012; Xiang et al. 2016). Moreover, inside curved and spiral microchannels, particles can be focused on one equilibrium position (Nivedita and Papautsky 2013; Nivedita et al. 2017; Chung 2019; Erdem et al. 2020; Huang et al. 2020; Chen et al. 2021). The net inertial lift force (F_L) represents the balance between the two dominant inertial forces as illustrated in Eq. 1 (Yuan et al. 2018).

$$F_L = \rho C_L \dot{\gamma}^2 a^4 \tag{1}$$

In Eq. 1, C_L represents the average lift coefficient (Yuan et al. 2018), and $\dot{\gamma} = 1.5V_x/D_h$ shows the average shear rate on channel walls (Martel and Toner 2012).

Due to the creation of secondary (Dean) vortices in curvilinear microchannels, particles experience an additional viscous drag in the lateral direction (Di Carlo 2009; Martel and Toner 2014). This Dean drag could further modify the particles focusing positions inside the microchannel. The modified particles' equilibrium positions depend on the relative strength of the Dean drag and the net inertial lift forces. The strength of secondary vortices is characterized using the non-dimensional Dean number as shown in Eq. 2 (Berger et al. 1983; Munson et al. 2009).

$$De = Re\sqrt{\frac{D_h}{2R}} \tag{2}$$

Here, R stands for the channel radius of curvature.

Particles could be focused close to the channel inner wall (closer to the center of curvature) under the dominant effect of inertial forces. However, larger and dominant Dean drags could entrain microparticles with the secondary vortices, which may result in particle dispersion across the channel cross section (Martel and Toner 2012, 2014). In curvilinear microchannels the Dean drag (F_D) could be presented as a function of the average secondary (Dean) vortex velocity (V_{De}) as shown in Eq. 3.

$$F_D = 3\pi \mu a V_{De} \tag{3}$$

Therefore, a thorough knowledge of the effects of fluid properties and channel dimensions on the average Dean velocity could facilitate a precise control over microparticle migration in curved microchannels (Bhagat et al. 2008; Kuntaegowdanahalli et al. 2009). There have been numerical (Ookawara et al. 2004; Martel and Toner 2013), and experimental (Bara and Masliyah 1992; Bayat and Rezai 2017) investigations on the average Dean velocity of Newtonian fluids. Later on, V_{De} estimations were used to design high throughput washing process in which microparticles were separated with high efficiencies (> 90%) and were transferred into a clean buffer (Bayat and Rezai 2018; Nikdoost et al. 2021).

In spite of reported investigations on the average Dean velocity in Newtonian fluids, many real-life applications deal with the fluids that exhibit non-Newtonian behaviors, i.e., shear thinning or thickening behaviors. For instance, in biological fluids (blood, saliva and urine) (Rafeie et al. 2016; Tian et al. 2018; Kim et al. 2021; Yan et al. 2022), and food applications [raw milk (Bienvenue et al. 2003)], fluid's rheological characteristics depend on the applied shear stress. Therefore, in curved microchannels, the balance between the inertial and elastic forces and the Dean drag determines the particle equilibrium positions (Del Giudice et al. 2013; Lim et al. 2014a, b; D'Avino et al. 2017; Faridi et al. 2017; Lu et al. 2017; Yang et al. 2017, 2019). Polymeric solutions such as polyethylene oxide (PEO) and polyvinylpyrrolidone (PVP) have been used to imitate these non-Newtonian fluids and investigate the particle behavior in microchannels. The effects of fluid viscosity and De number on the Dean velocity of these shear-thinning fluids have been numerically studied by Yoon et al. (2020a; b), Ducloué et al. (2019) and others (Norouzi et al. 2010; Vamerzani et al. 2014; Sprenger et al. 2015). We reported an experimental investigation of the effects of fluid properties and channel dimensions on the average V_{De} in PEO solutions in curved microchannels (Nikdoost and Rezai 2020), and offered an empirical correlation with an accurate estimation of V_{De} in viscoelastic PEO solutions as shown in Eq. 4.

$$Re_{V_{De}} = \frac{V_{De}D_h}{\vartheta} = 0.01\,De^{1.89} \tag{4}$$

Here, $\vartheta = \mu/\rho$ is the fluid kinematic viscosity.

Microparticle manipulation in shear-thinning fluids inside the spiral and curvilinear microchannels have been reported by Raoufi et al. (2021), Narayana Iyengar et al. (2021), and Kumar et al. (2021) and others (Lee et al. 2013; Xiang et al. 2016; Yuan et al. 2019; Fan et al. 2020; Zhou et al. 2020; Feng et al. 2022). We recently reported a fundamental investigation of microparticle focusing behavior in viscoelastic fluids inside curved microchannels at high flow rates (up to 2 ml/min) (Nikdoost and Rezai 2022b). We examined the particle dynamics for different particle sizes and reported on the effects of fluid viscosity, and channel width, height and radius of curvature in a co-flow of PEO solutions inside a curved microchannel. Moreover, utilizing our empirical correlation for the average V_{De} of PEO solutions (Eq. 4), a proof of concept demonstrations of duplex particle separation and washing was presented. Recent reports on the fundamentals of elasto-inertial particle focusing could be found elsewhere (Xiang et al. 2016; Yuan et al. 2018; Zhou and Papautsky 2020).

To paint a complete picture of various non-Newtonian fluid types, and based on our interest in studies of particle dynamics inside curved microchannels, we have focused our attention towards mixtures of metallic nanoparticles with water (Nakanishi et al. 2012). These colloidal suspensions exhibit a drastic increase in viscosity as the shear rate increases (Boersma and Stein 1990; Lee and Wagner 2003, 2006; Wagner et al. 2009). Under deformation, the randomly dispersed nanoparticles in the medium shape into layered structures, which cause a shear-thinning behavior at lower shear rates. However, beyond a critical shear rate threshold, these layered structures form hydroclusters and cause a drastic viscosity increase (Hasanzadeh et al. 2014). Rheological characteristics of these fluids depend on several factors such as the liquid medium, particles, particle interactions, temperature, etc. (Gürgen et al. 2017). For instance, Moldaveanu et al. (2018) investigated the rheological characteristics of metallic Al_2O_3 and SiO_2 nanofluids and offered few correlations for a better estimation of their viscosity over a wide range of shear rates.

Initially, we investigated the average Dean velocity of SiO_2 nanofluids in curved microchannels and reported a modified correlation for V_{De}, which significantly improved the V_{De} estimation as shown in Eq. 5 (Nikdoost and Rezai 2022a).

$$Re_{V_{De}} = \frac{V_{De}D_h}{\vartheta} = 0.08De^{1.88}\left(\frac{\vartheta}{\vartheta_{water}}\right)^{0.90} \tag{5}$$

This correlation can be used to design more accurate microparticle sorting and washing devices in shear-thickening fluids inside curved microchannels. We envision a near future application for these nanofluids, such as the suspensions of SiO_2 nanoparticle in water, for microparticle manipulation in microfluidic devices for various thermal and energy applications.

Utilizing the developed correlation (Eq. 5) for the average Dean velocity of SiO_2 nanofluids, in here we aimed to propose a novel experimental study on the particle behavior in these fluids. It is worth noting that as opposed to shear-thinning fluids, there is a lack of knowledge on the governing non-dimensional numbers (i.e., *Weissenberg* and *Elasticity*) to characterize the shear-dependent effects and the hydrodynamic forces acting on the particles. We are pursuing fundamental research to improve understanding of the particle migration in our experiments. In this paper, particle migration is described using the available non-dimensional numbers (*Re* and *De*), and the balance between net inertial lift force and the Dean drag. Early investigations on particle behavior in SiO_2 nanofluids in our group (Charjouei Moghadam 2021) indicated that inside a straight microchannel, particles tend to occupy two focusing lines on the channel sides at lower axial velocities where the effect of inertial focusing is not significant. Moreover, at higher axial velocities (i.e., larger *Re* numbers), the particles migration in SiO_2 nanofluids were comparable to inertial focusing in water, where three focusing lines were observed in a square microchannel. Here, for the first time we present the particle migration behavior in co-flows of SiO_2 nanofluids inside curved microchannels. The normalized lateral positions of microparticles are used to describe the effects of fluid axial velocity, nanofluids concentration, channel width and radius of curvature, and particle size.

2 Materials and methods

2.1 Sample preparation

The nanofluids were prepared using the colloidal dispersion of SiO_2 (40% in water, Alfa Aesar, USA) with previously reported viscosities (Moldoveanu et al. 2018) at three different concentrations of $\varphi = 1\%$, 2%, and 3% v/v. Viscosity estimations as a power function of the shear rate are presented in the supplementary material. As given by the manufacturer, the solutions were prepared using SiO_2 nanoparticles with an average size of 20 nm. Three different microparticle sizes of 10.6 µm (~ 10 µm, CM-100–10, 1% w/v), 14.5 µm (~ 15 µm, CM-150–10, 1% w/v), and 22 µm (CM-200–10, 1% w/v) were obtained from Spherotech Inc., USA. Microparticle solutions were prepared at an approximate particle concentration of 2×10^5 particles/ml with 0.5% v/v Tween 20 (Sigma Aldrich, USA) to prevent particle aggregation.

2.2 Microfluidic device

Photolithography technique was used to prepare the master molds for straight (Fig. 1a) and curved (Fig. 1b) microchannels. Initially, a layer of SU-8 2075 photoresist (MicroChem Corp., USA) was spin-coated on 4 inch silicon wafers (Wafer World Inc., USA). This was followed by prebaking at 65 °C and 95 °C, and the UV light exposure (UV-KUB 2, KLOE, France) using different photomask designs. Next, a post-bake process at 65 °C and 95 °C was applied, and later, silicon master molds were developed in SU-8 developer and underwent a hard-bake at 200 °C.

Microdevices were prepared in polydimethylsiloxane (PDMS, Sylgard 184 silicone elastomer kit, Dow Corning, Canada) using the soft lithography technique (Xia and Whitesides 1998). PDMS prepolymer and the curing agent were mixed at 10-to-1 ratio, casted over the master molds, and baked at 75 °C for 3 h. Finally, the PDMS replicates were bonded onto glass slides using oxygen plasma (Harrick Plasma Inc., USA).

As illustrated in Fig. 1b, our curved microchannels consisted of two inlets to supply the particles (inlet-I) alongside

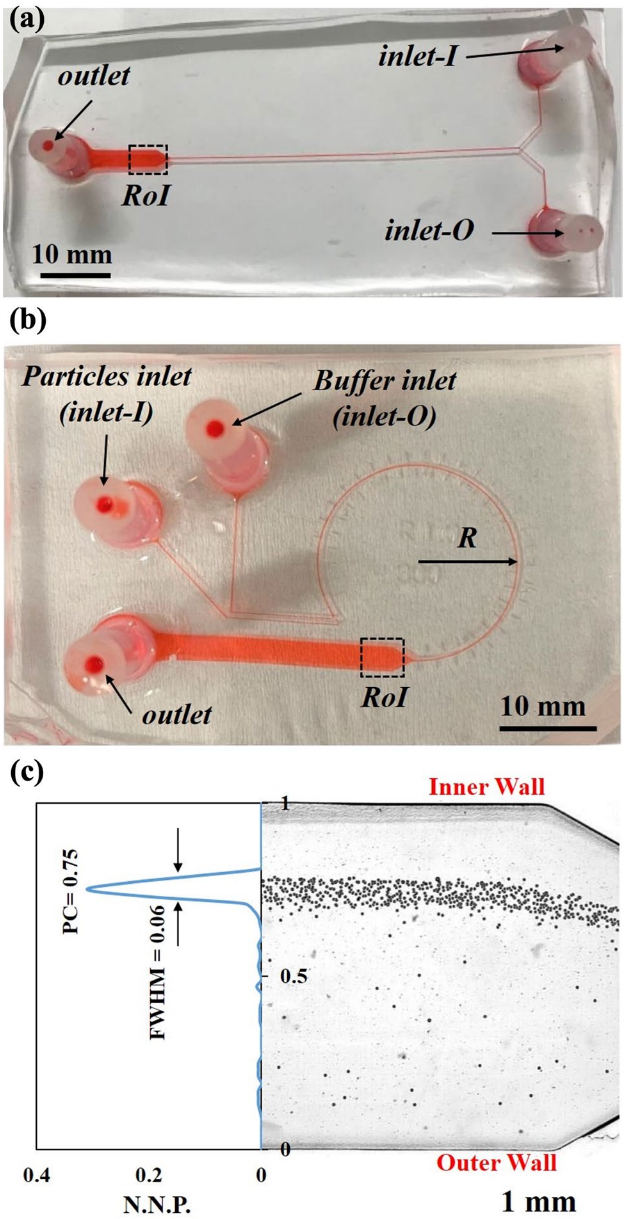

Fig. 1 Microfluidic devices for investigation of particle focusing behavior in SiO_2 nanofluids. Microchannels include two inlets to supply the particles (inlet-I) and a clean buffer (inlet-O), and an expanded outlet ($w = 2.55$ mm) for particle visualization. **a** Straight microchannel with a length of ~ 5.23 cm. **b** A curved microchannel with a constant radius of curvature $R = 1.0$ cm, a 300° curvature, and a cross section of $w \times h = 150 \times 150$ μm^2. **c** Particles trajectories at the Region of Interest [RoI in (b)] for $a = 22$ μm particles in $\varphi = 3\%$ v/v SiO_2 nanofluids at a total axial velocity of $V_x = 0.148$ m/s. NNP (normalized number of particles) are drawn alongside the normalized channel width. FWHM represents the full width at half maximum, and PC stands for the peak centroid in particle distribution

a clean buffer (inlet-O), into a 300° curved microchannel with a constant radius of curvature, R. An expanded outlet with a width of $w = 2.55$ mm was designed to enable the particle visualization at a lower axial speed. Three different microchannel widths of $w = 150$, 225, and 300 μm were used to capture the effect of channel width at a constant height of $h = 150$ μm. To investigate the effect of channel curvature, square microchannels (150×150 μm^2) were fabricated with three different radii of curvature of $R = 1.0$, 1.5, and 2.0 cm, with a constant channel length (300°, 225°, and 150° curvatures, respectively). As shown in Fig. 1a, a straight microchannel (150×150 μm^2) with similar channel length (~ 5.23 cm) was used to investigate the particles focusing behavior in straight microchannels and comprehensively study the effect of channel curvature.

2.3 Experimental procedure

Particles focusing behavior was initially investigated in the straight channel (Fig. 1a), where microparticles in various SiO_2 concentrations were supplied through both inlets (inlet-I and inlet-O). Later on, microparticles focusing behavior was analyzed using a co-flow of SiO_2 nanofluids (one with particles at inlet-I and one clean buffer at inlet-O) at total flow rates of $0.05 < Q_t < 1.5$ ml/min (i.e., 0.025–0.75 ml/min in each inlet). These flow rates translate to average axial velocities of $0.037 < V_x < 1.11$ m/s (i.e., 0.0185–0.555 m/s in each inlet) in the square microchannel (150×150 μm^2). Microparticle trajectories at the channel outlet (Fig. 1c) were recorded on an inverted microscope (Bioimager, BIM 500 FL, Canada) at 2.5 × magnification using a high speed camera (FASTEC IL 5, Canada) at different frame rates (28–1400 fps with respect to the average axial velocity). Each experiment was repeated two times, and the images were analyzed using the open source ImageJ software (Abràmoff et al. 2004; Schneider et al. 2012) as thoroughly explained below.

2.4 Data analysis

The WrMTrck plugin (Nussbaum-Krammer et al. 2015) in ImageJ (Abràmoff et al. 2004; Schneider et al. 2012) was used to analyze the particle trajectories frame by frame. Figure 1c shows the overlap of microparticles trajectories, where particles' lateral position alongside the channel length is normalized. Here, 0 refers to the channel outer wall and 1 indicates the channel inner wall (i.e., close to the center of curvature). Initially, the backgrounds were subtracted from the image stacks, and then the color intensities were adjusted to obtain a black and white stack to trace the particles using the WrMTrck plugin. Particle distributions were obtained by dividing the outlet width into 50 equal sections. This discretization provided a higher resolution compared to the smallest particle size to the channel width ratio. As illustrated in Fig. 1c, the normalized number of particles (NNP) with respect to the total observed particles were drawn along the particles normalized lateral position. OriginPro (Origin 2022b, OriginLab Corp., USA) was used to analyze the particles distribution and obtain the number of peaks, peak centroids (PC), and the full width at half maximum (FWHM).

Focusing behaviors were categorized using the fraction of the NNP within a ± 0.1 normalized bandwidth around each peak centroid. Normalized number of particles fractions higher than 90%, were identified as full focusing, while a partial focusing was defined as NNP fractions between 70 and 90%. NNP fractions less than 70% within the ± 0.1 bandwidth were categorized as no focusing behavior. Particle distributions with multiple peaks were categorized individually based on the total number of peaks.

Fluid recirculation in curved microchannels could be estimated using our previously reported correlation for the average V_{De} of SiO_2 nanofluids (Eq. 5). The average V_{De} was predicted for each experiment and used to obtain the required channel length for one fluid switch (L_s, where $L_s = L_R V_x / V_{De}$) (Nikdoost and Rezai 2020). Here, the fluid's average lateral migration (L_R) could be estimated as $L_R = 0.75\ D_h$ (Martel and Toner 2012). Since the curved channel length remains constant for all radii of curvatures ($L_{curve} = 5.23$ cm), the total number of fluid switches could be approximated by the ratio of L_{curve}/L_s. The number of fluid switches could be used to estimate the lateral position of particles under the sole effect of Dean drag force.

3 Results and discussion

Particle migration in curvilinear channels was investigated for three different particle sizes (~ 10, 15, and 22 µm) inside co-flows of various SiO_2 nanofluids concentrations (φ = 1%, 2%, and 3% v/v). Straight (Fig. 1a) and curvilinear (Fig. 1b) microchannels with different channel widths, and radii of curvature were used to study the effects of channel geometry and channel curvature. As explained earlier, particle trajectory videos were used to obtain the normalized particle distribution (NNP) alongside the channel width, and find the focusing peaks location, peak centroids (PCs), and the full width at half maximum (FWHM), which represents the particles distribution bandwidths.

Initially, we investigated the particles behavior in a straight microchannel, once injected from both inlets and once injected from one inlet just like the curved microchannels. First, particles were supplied through both inlets of the straight channel (Fig. 1a). As represented in Fig. 2a, the 15 µm particles in DI water at an axial velocity of $V_x = 0.222$ m/s inside this square straight microchannel (150 × 150 µm^2) occupied three inertial focusing locations ($PC_{a1} = 0.13$, $PC_{a2} = 0.49$, $PC_{a3} = 0.77$), with the majority of particles (~ 50%) close to the channel center. Similarly, inside the 2% v/v SiO_2 nanofluid (Fig. 2b), particles occupied three focusing locations ($PC_{b1} = 0.15$, $PC_{b2} = 0.49$, $PC_{b3} = 0.79$). However, inside the SiO_2 nanofluids, a more uniform particle distribution was achieved alongside the channel width, where around 30% of particles were found within a ± 0.1 bandwidth of each respective peak.

Next, 15 µm particles were supplied into the straight microchannel in one inlet alongside a clean buffer in the other inlet. As shown in Fig. 2c, microparticles in DI water were mainly gathered close to where they were supplied at the channel inner side with a peak centroid of $PC_c = 0.81$ and $FWHM_c = 0.06$. However, inside the 2% v/v SiO_2 nanofluids, microparticles were dispersed alongside the channel width with two apparent peak centroids of $PC_{d1} = 0.57$ ($FWHM_{d1} = 0.06$), and $PC_{d2} = 0.87$ ($FWHM_{d2} = 0.18$) as shown in Fig. 2d. Here, the particles in DI water were partially focused (~ 86% within the ± 0.1 peak bandwidth), while ~ 42% of particles were accumulated within ± 0.1 peak bandwidth around each peak inside the 2% v/v SiO_2 nanofluids. Obviously, the SiO_2 nanofluid exerted a distracting effect on particle focusing in the straight microchannel.

To investigate the effect of channel curvature, microparticles were supplied inside a channel with $R = 1.0$ cm and a square cross section (150 × 150 µm^2). As represented in Fig. 2e, the DI water recirculation ($De = 3.21$, and ~ 3.1 fluid switches) resulted in particles dispersion at the channel outlet, where ~ 54% of particles were found around the $PC_e = 0.75$, with an $FWHM_e = 0.09$. However, as shown in Fig. 2f, the Dean drag (~ 1.4 fluid switches with $De = 0.06$) transferred the particles inside the 2% SiO_2 towards the outer wall with two weak peaks ($PC_{f1} = 0.13$, $FWHM_{f1} = 0.11$, and $PC_{f2} = 0.77$, $FWHM_{f2} = 0.14$). Here, ~ 32%, and 27% of particles were found within the ± 0.1 peak bandwidth for the first and second peak, respectively. We concluded again that (1) the addition of Dean drag with a curvilinear microchannel scattered the particle trajectories inside DI water, and (2) the addition of SiO_2 nanoparticles changed the behaviour of particles inside the curved microchannel.

The outcomes of the above preliminary investigations encouraged us to conduct a parametric study on particle focusing inside SiO_2 nanofluids in curved microchannels. The results are presented in the following sections.

3.1 Effect of fluid axial velocity (V_x)

Particle migration behavior was studied at a wide range of axial velocities between $0.037 < V_x < 0.74$ m/s inside curved microchannels with square cross sections (150 × 150 µm^2) and $R = 1.0$ cm. Figure 3 illustrates the focusing behavior of 22 µm particles in co-flows of 3% v/v SiO_2 nanofluids inside this curved microchannel. Here, at an axial velocity of $V_x = 0.037$ m/s ($De = 0.034$, ~ 0.3 fluid switch), particles were fully focused close to the channel inner wall, with ~ 90% of particles within the ± 0.1 bandwidth of peak centroid

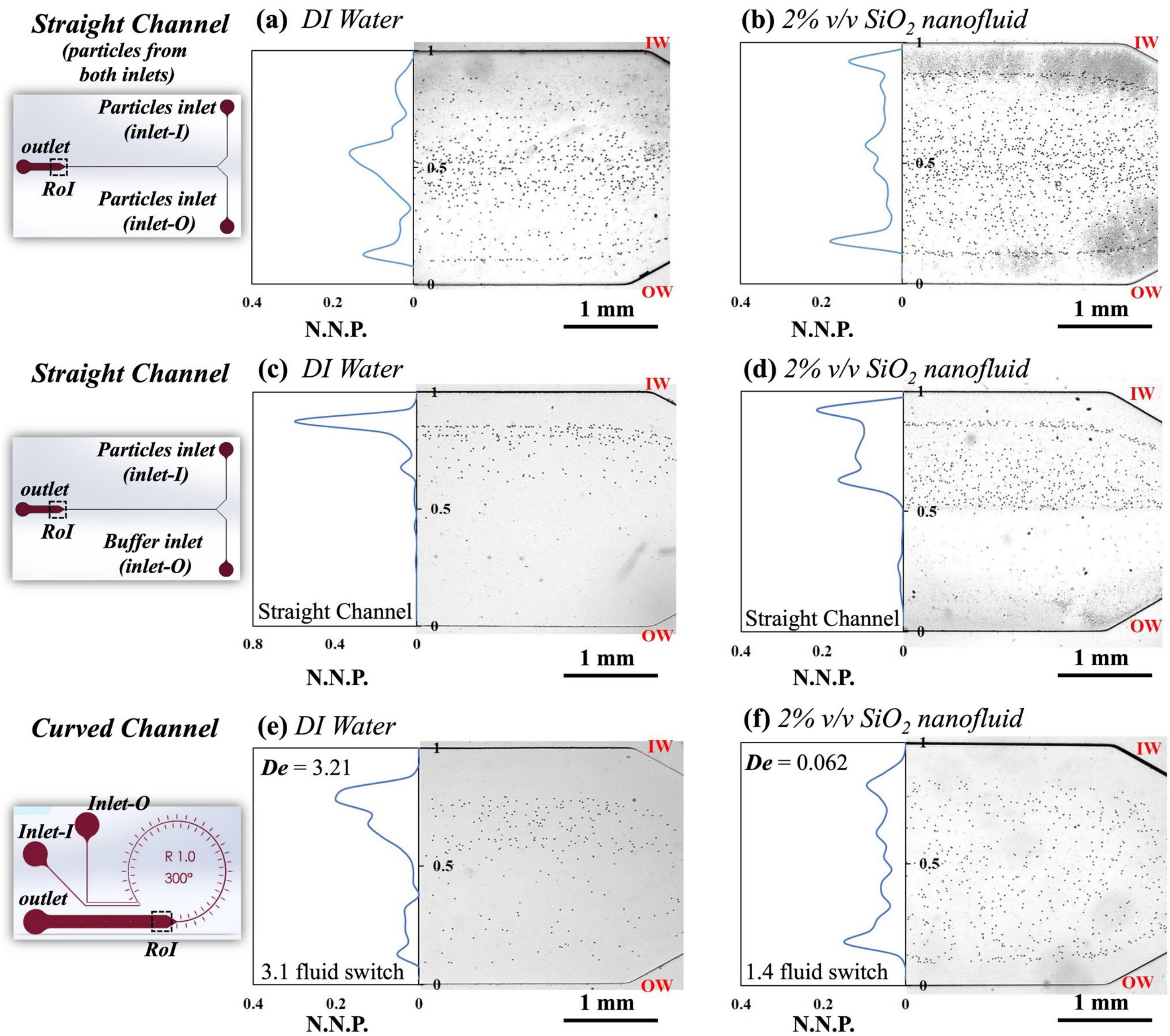

Fig. 2 Particle trajectories and normalized number of particles (NNP) across the RoI of the channels for 15 µm particles at an axial velocity of $V_x = 0.222$ m/s inside square microchannels (150×150 µm^2). Particles were supplied through both inlets in **a** DI water, and **b** 2% v/v SiO_2 nanofluids inside a straight channel. Particles were co-flown alongside a clean buffer inside a straight channel in **c** DI water and **d** 2% v/v SiO_2 nanofluids, and inside a curved channel with $R = 1.0$ cm in **e** DI water, and **f** 2% v/v SiO_2 nanofluids

(PC = 0.81). As the axial velocity increased to $V_x = 0.074$ m/s (~0.5 fluid switch), and $V_x = 0.148$ m/s (~1 fluid switch), the peak centroids shifted insignificantly towards the channel center (PC = 0.79, and PC = 0.75, respectively), due to the higher fluid recirculation. Here, approximately 85% of particles were found within the ± 0.1 bandwidth around the peaks (i.e. partially focused) for both axial velocities. Upon further increase in axial velocity, the Dean drag dominated the particle migration. For instance, at $V_x = 0.222$ m/s, only ~48% of particles were found within the ± 0.1 bandwidth around PC = 0.81 (no focusing). At higher axial velocities of $V_x = 0.37$ m/s to $V_x = 0.74$ m/s, two weak peaks appeared in particle distribution close to channel walls (PC = 0.17, and PC = 0.77). It could be observed that stronger Dean vortices at higher axial velocities resulted in particle dispersion along the channel width, while other forces such as inertia helped forming insignificant peaks.

3.2 Effect of SiO_2 concentration

Preliminary experiments (Fig. 2) indicated behavioral changes in particle focusing in SiO_2 nanofluids compared to DI water. Here, different concentrations of SiO_2 nanofluids (φ = 1%, 2%, and 3% v/v) were examined to investigate the

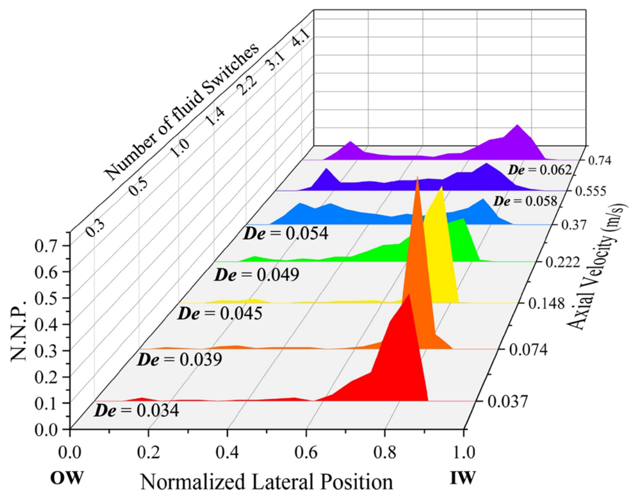

Fig. 3 Normalized number of particles alongside their normalized lateral position for 22 μm particles in 3% SiO_2 nanofluid inside a square microchannel (150 × 150 μm^2) with $R = 1.0$ cm at various axial velocities

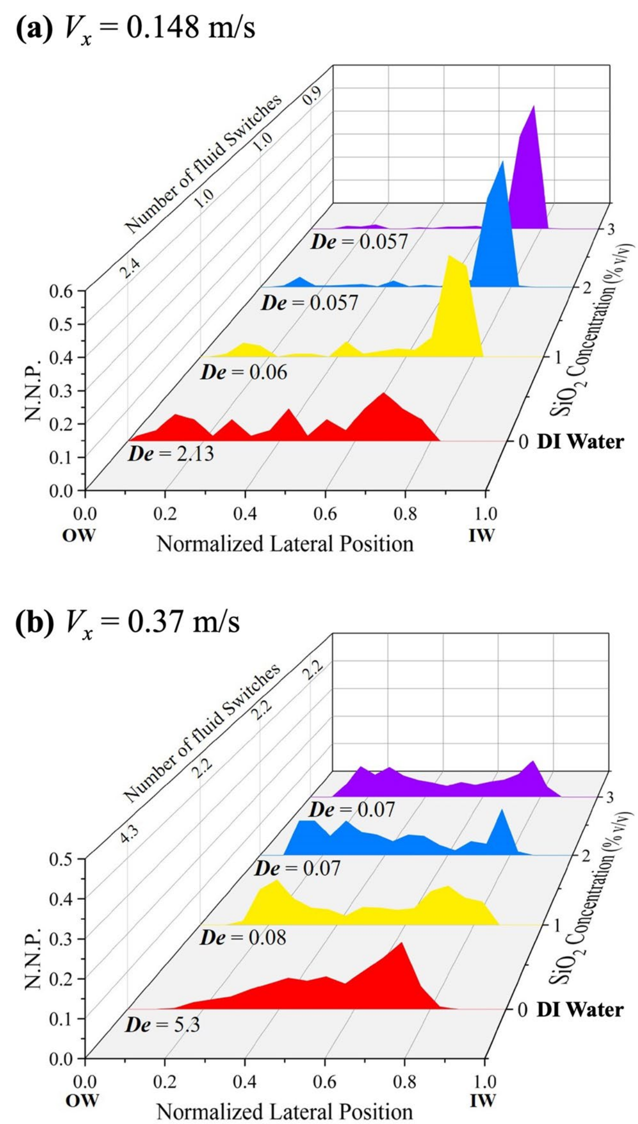

Fig. 4 Normalized number of particles alongside their normalized lateral position for 22 μm particles in a square microchannel (150 × 150 μm^2) with $R = 1.0$ cm in DI water, and 1%, 2%, and 3% v/v SiO_2 nanofluids at **a** $V_x = 0.148$ m/s, and **b** $V_x = 0.37$ m/s

shear-dependent effect on particle migration. Representative experiments for 22 μm particles in curved microchannel with a square cross section of 150 × 150 μm^2, and $R = 1.0$ cm at two different axial velocities are presented in Fig. 4.

As shown in Fig. 4a, at an axial velocity of $V_x = 0.148$ m/s, particles in DI water ($De = 2.13$) were dispersed across the channel width after the second fluid switch. As the SiO_2 nanofluids were introduced, the fluid switches reduced to ~ 1 and microparticles remained close to the channel inner wall. Here, the added effect of the nanofluid and the increased dominance of the Dean drag ($F_D > F_L$) at higher fluid viscosities, resulted in particle focusing at a peak centroid of PC = 0.75 for all three concentrations. For the co-flow of φ = 1%, and 2% v/v SiO_2 ($De = 0.06$ and 0.057, respectively), particles were partially focused with ~ 73%, and ~ 83% of them within the ± 0.1 bandwidth of the peak centroid, respectively. However, at a higher concentration of φ = 3% v/v, particles were fully focused around the PC = 0.75 (~ 90% within the defined bandwidth).

Particle distributions are also shown at a higher axial velocity of $V_x = 0.37$ m/s in Fig. 4b. Here, inside DI water ($De = 5.3$, and ~ 4.3 fluid switches) particles were scattered across the channel width with only ~ 40% of them found within the ± 0.1 bandwidth of PC = 0.73. For particles in 1% v/v SiO_2 ($De = 0.08$, and ~ 2.2 fluid switches), two peaks were observed at $PC_1 = 0.23$, and $PC_2 = 0.81$, with ~ 37%, and 26% of particles within their respective bandwidths. For higher SiO_2 concentrations (φ = 2%, and 3% v/v), particles were pushed towards the channel walls with $PC_1 = 0.15$, and $PC_2 = 0.77$, and only ~ 30% of particles within each peak's defined bandwidth. Here, we concluded that shear-dependent effect of SiO_2 nanofluids would enhance the particle focusing at lower axial velocities (Fig. 4a). However, at higher axial velocities the dominant Dean drag leads to particle scattering and creation of two main peaks close to the channel walls (Fig. 4b).

3.3 Effect of channel radius of curvature (R)

To investigate the effect of channel curvature, 22 μm particles were co-flown in various SiO_2 concentrations inside curved microchannels with square cross sections and $R = 1.0$, 1.5, and 2.0 cm. Experiments for straight channels ($R \to \infty$) were also conducted for comparison purposes. As an example, the normalized particle distributions alongside the channel width in co-flows of 3% v/v SiO_2 nanofluids at two different axial velocities of $V_x = 0.37$ m/s and $V_x = 0.74$ m/s are presented in Fig. 5.

As shown in Fig. 5a, inside a straight microchannel at an axial velocity of $V_x = 0.37$ m/s, microparticles occupied two peaks close to the channel inner wall and channel center line ($PC_1 = 0.53$, and $PC_2 = 0.87$), where ~ 40% and 56% of particles were within the ± 0.1 bandwidth of each respective peak centroid. As a reminder, this behavior was due to the supply of the particles only from one of the two inlets into the straight microchannel. Upon introduction of channel curvature (and Dean drag) inside a curved channel with $R = 2.0$ cm (~ 1.1 fluid switch), particles were partially focused (~ 86% within the defined bandwidth) close to the inner wall with PC = 0.85. As the channel radius of curvature decreased to $R = 1.5$ cm (~ 1.5 fluid switches), particles were pushed towards the channel center, where they were partially focused (~ 85% within the defined bandwidth) with a peak centroid of PC = 0.75. A further decrease in channel radius of curvature to $R = 1.0$ cm, resulted in ~ 2.2 fluid switches and dispersed the particles across the channel width with two peaks close to the side channels ($PC_1 = 0.15$, and $PC_2 = 0.77$).

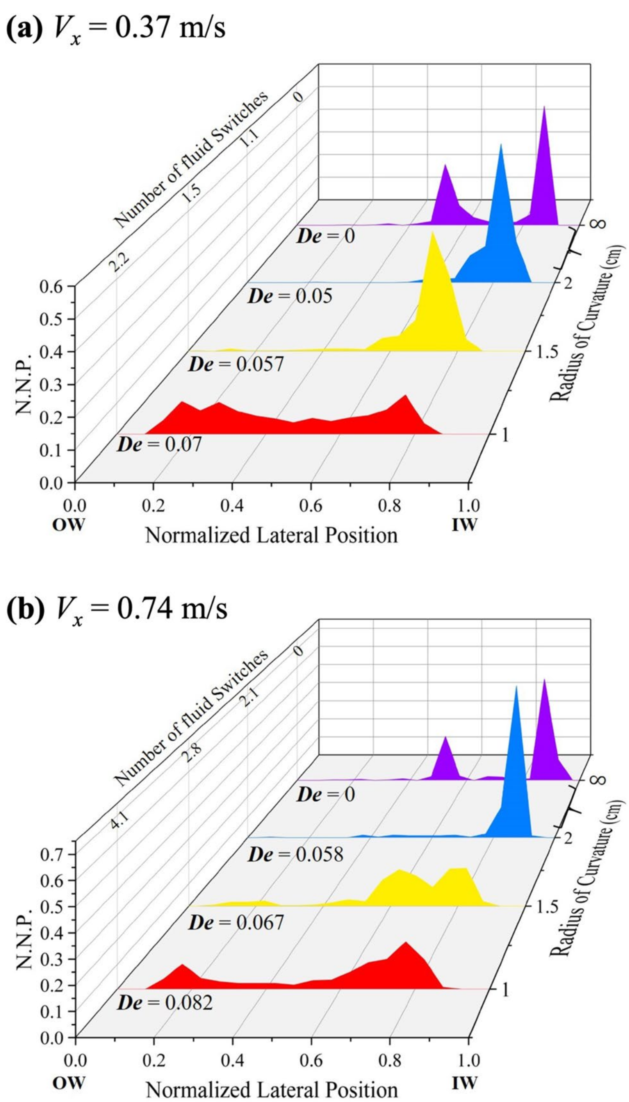

Fig. 5 Effect of radius of curvature on normalized number of particles alongside the channel outlet. Representative experiments are shown for 22 µm particles in co-flow of 3% v/v SiO_2 nanofluids inside the straight ($R \rightarrow \infty$) and curved microchannels with $R = 1.0$, 1.5, and 2.0 cm with a square cross section (150×150 µm^2) at an axial velocity of **a** $V_x = 0.37$ m/s, and **b** $V_x = 0.74$ m/s

The normalized lateral migration of particles at a higher axial velocity of $V_x = 0.74$ m/s is also presented in Fig. 5b. Here, inside a straight microchannel ($R \rightarrow \infty$), two peaks were observed at $PC_1 = 0.51$, and $PC_2 = 0.89$, with ~ 28% and ~ 66% of particles within their respective ± 0.1 bandwidths. As shown in Fig. 5b, particles inside a curved channel with $R = 2.0$ cm were fully focused close to the channel inner wall, where ~ 92% of them were within the defined bandwidth around PC = 0.87. Further decrease in channel radius of curvature to $R = 1.5$ cm, resulted in the creation of two peaks ($PC_1 = 0.67$, and $PC_2 = 0.87$) with an approximate 3 fluid switches at the channel outlet. Here, ~ 45% of particles were found within the ± 0.1 bandwidth of each peak. A further decrease in channel radius of curvature to $R = 1.0$ cm (~ 4 fluid switches) amplified the effect of Dean drag and pushed the particles towards side channels with two apparent peaks of $PC_1 = 0.15$, and $PC_2 = 0.75$, with ~ 19% and 50% of particles within their respective bandwidths.

According to the representative cases in Fig. 5, we concluded that at lower channel curvatures (higher R values), the added effect of Dean drag could enhance the particle focusing, i.e., resulting transition from two peaks in straight channels into a single peak in a curved channel with SiO_2 nanofluid. However, stronger Dean vortices at lower channel radii would disperse the particles towards channel walls. At higher axial velocities, this phenomenon would occur faster at a higher channel radius of curvatures.

3.4 Effect of channel width (w)

The effect of channel width on particle migration was investigated using curved microchannels with $R = 1.0$ cm at three different channel width of $w = 150$, 225, and 300 µm with a constant height of $h = 150$ µm. Figure 6 shows the representative experiments for $a = 15$ µm particles in a co-flow of 3% v/v SiO_2 nanofluids at two different axial velocities of $V_x = 0.222$ m/s and 0.37 m/s.

As shown in Fig. 6a, at $V_x = 0.222$ m/s inside the curved channel with $w = 150$ µm (~ 1.5 fluid switch with $De = 0.062$), microparticles were distributed close to the channel walls with two apparent peaks of $PC_1 = 0.15$ ($FWHM_1 = 0.07$), and $PC_2 = 0.73$ ($FWHM_2 = 0.16$). Here, the relatively strong

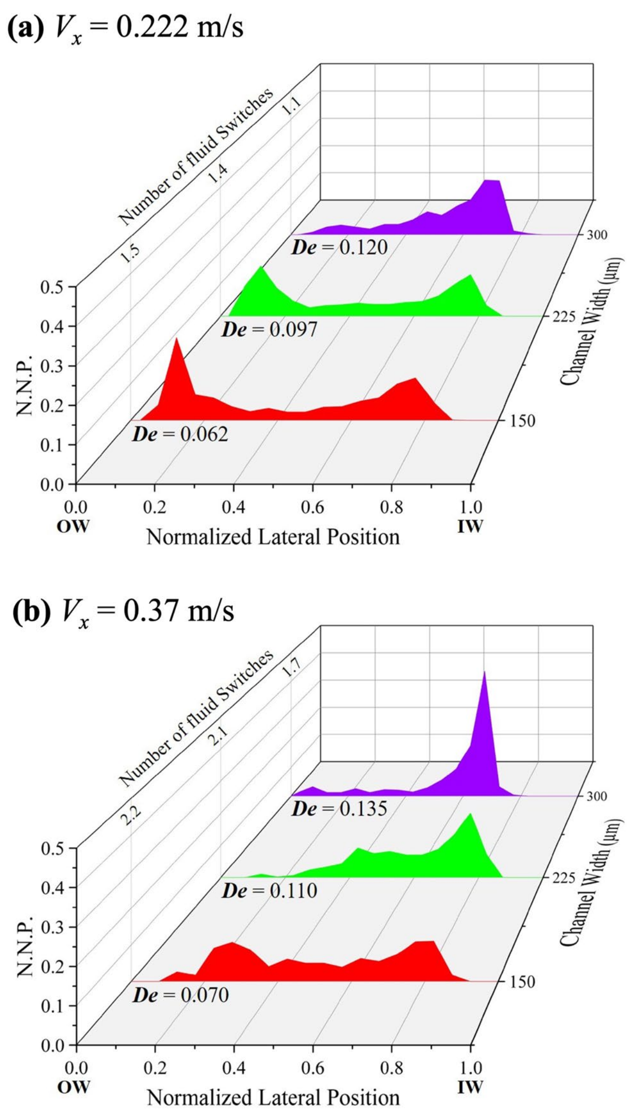

Fig. 6 Effect of channel width on normalized number of particles alongside the channel outlet. Representative experiments are shown for 15 μm particles in co-flow of 3% v/v SiO_2 nanofluids inside curved microchannels with $R = 1.0$, a constant channel height of $h = 150$ μm, and three channel widths of $w = 150$ μm, 225 μm, and 300 μm at an axial velocity of **a** $V_x = 0.222$ m/s, and **b** $V_x = 0.37$ m/s

Dean drags alongside the effect of SiO_2 nanofluid pushed the particles into two focusing peaks, where ~ 40% and ~ 33% of particles were found within the ± 0.1 bandwidth of the first and second peak, respectively. Inside a rectangular channel with a width of $w = 225$ μm (~ 1.4 fluid switch with $De = 0.097$), microparticles occupied two focusing peaks close to the walls with $PC_1 = 0.15$ ($FWHM_1 = 0.12$), and $PC_2 = 0.69$ ($FWHM_2 = 0.1$) with similar distributions compared to a channel with $w = 150$ μm. As the channel width increased to $w = 300$ μm (~ 1.1 fluid switch with $De = 0.12$), the effect of Dean drag degraded and particles remained closer to the channel center and the inner wall, with ~ 61% particles found within the ± 0.1 bandwidth of PC = 0.59 (FWHM = 0.16). Increasing the channel width translates into higher hydraulic diameters ($D_h = 150$, 180, and 200 μm), which results in a lower shear rate and a lower fluid viscosity at a constant axial velocity. Therefore, despite the increase in the Dean number, the effect of viscous drag forces would reduce, and particles remain mainly close to the inner wall for the highest channel width.

At a higher axial velocity of $V_x = 0.37$ m/s, particles in the square microchannel ($w = 150$ μm) were dispersed alongside the channel width under the effect of strong Dean drags (~ 2.2 fluid switches with $De = 0.07$). Here, around 33% of particles were found within the respective bandwidths of $PC_1 = 0.35$ ($FHWM_1 = 0.16$), and $PC_2 = 0.74$ ($FWHM_2 = 0.15$). As the width increased to $w = 225$ μm (~ 2.1 fluid switches with $De = 0.11$), the second peak centroid started to vanish as the Dean drag effect degraded. Here, approximately 44% of particles were found within the ± 0.1 bandwidth around the PC = 0.74 (FWHM = 0.13), as the majority of particles remained close to the inner wall despite two fluid switches. Finally, at the largest channel width of $w = 300$ μm (~ 1.7 fluid switches with $De = 0.135$), the reduced effect of Dean drag did not disturb the particle focusing around the PC = 0.64 (FWHM = 0.07), where ~ 75% of particles were found within the respective bandwidth (i.e., partially focused).

Based on the representative cases in Fig. 6, lower Dean drags could improve the particle focusing close to the channel inner wall. As the Dean drag increases in the lower channel widths, particles were dispersed into two focusing peaks alongside the channel. At a constant axial velocity, the fluid viscosity drops as the channel width increases. Therefore, higher channel widths works against the dominance of Dean drag, despite the increase in Dean number, and a constant trend was not observed in our representative experiments.

3.5 Effect of microparticle size (a)

Finally, the effect of particle size was investigated using three different particle sizes of 10, 15, and 22 μm in a curved microchannel with square cross section (150 × 150 μm^2) and $R = 1.0$ cm. Representative cases for microparticles in co-flows of 3% v/v SiO_2 nanofluids at two different axial velocities are presented in Fig. 7.

As shown in Fig. 7a, at an axial velocity of $V_x = 0.148$ m/s (~ 1 fluid switch) the smaller 10 μm particles ($\beta = 0.07$) were scattered across the channel width with two peaks of $PC_1 = 0.33$, and $PC_2 = 0.71$, with ~ 30% of particles within the ± 0.1 bandwidth around each peak. As the particle size increased to 15 μm ($\beta = 0.1$), the net inertial lift forces ($F_L \sim a^4$ in Eq. 1) increased faster compared to the Dean drag ($F_D \sim a$ in Eq. 3). Therefore, the particles were pushed towards the channel inner wall with PC = 0.59, with ~ 53% of

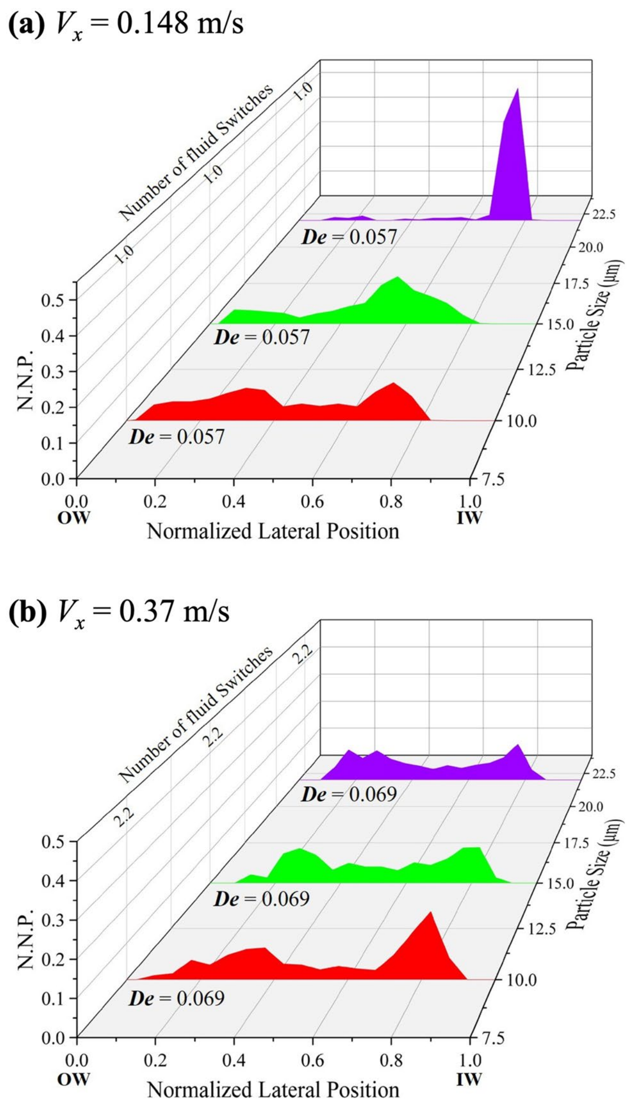

Fig. 7 Effect of particle size on normalized number of particles alongside the channel outlet. Representative experiments are shown for three different particle sizes of 10, 15, and 22 µm microparticles in co-flow of 3% v/v SiO_2 nanofluids inside a microchannel with a 150×150 µm^2 cross section and $R = 1.0$ cm at **a** $V_x = 0.148$ m/s, and **b** $V_x = 0.37$ m/s

them within the defined bandwidth (no focusing). However, the larger 22 µm particles ($\beta = 0.15$) were fully focused close to the channel inner wall with ~ 92% of the particles found within the defined bandwidth surrounding PC = 0.81. As shown in Fig. 7b, at a higher axial velocity of $V_x = 0.37$ m/s (~ 2.2 fluid switches), microparticle migration was dominated by the Dean drag, and particles were scattered across the channel width with two weak peaks close to channel side walls for all particle sizes ($PC_1 = 0.25$, and $PC_2 = 0.75$).

Overall, we concluded that an increase in particle size could enhance the focusing behavior at lower axial velocities. However, as the Dean drag becomes dominant at higher axial velocities, all particles get dispersed in two main peaks close to the channel sidewalls.

4 Conclusion

In summary, we demonstrated the particle focusing behavior in SiO_2 nanofluids inside curved microchannels for the first time. The normalized lateral positions of particles were studied in co-flows of various SiO_2 nanofluid concentrations. The effects of fluid axial velocity, nanofluids concentration, channel width and radius of curvature, and particle size on the particle focusing at the channel outlet were investigated. We found out that the presence of nanofluids even at low concentrations, could enhance the particle focusing at lower flow rates. Moreover, the dominance of Dean drag at higher axial velocities (i.e., flow rates) would create two focusing peaks close to channel sidewalls. Our early results indicate a behavioral change and warrant a more comprehensive parametric study on this phenomenon in higher nanofluids concentrations, and different channel geometries at very low to very high flow rates. The parametric study should also include a non-dimensional analysis to extend its usefulness for future applications of these non-Newtonian fluids in heat exchangers, solar energy collectors, and nanoplastic detection in the food, energy, electronics, and environmental monitoring industries.

Supplementary Information The online version contains supplementary material available at https://doi.org/10.1007/s10404-023-02700-0.

Acknowledgements This study was funded by the Ontario Ministry of Agriculture, Food and Rural Affairs (OMAFRA 2018-0289) to PR, through the Ontario Agri-Food Innovation Alliance.

Author contributions P.R. developed the idea, provided funding, supervised the project, reviewed the results, interpreted the data, revised the paper, and oversaw the research project toward publication. A.N. matured the idea, performed experiments, analyzed the results, interpreted the data, wrote the first draft of the paper, and revised the paper.

Data availability The data that support the findings on this study are available from the corresponding author upon reasonable request.

Declarations

Conflict of interest The authors have no conflicts to disclose.

References

Abràmoff MD, Magalhães PJ, Ram SJ (2004) Image processing with imageJ. Biophoton Int 11(7):36–41. https://doi.org/10.1201/9781420005615.ax4

Bara B, Masliyah JH (1992) An experimental and numerical study of the Dean problem: flow development towards two-dimensional multiple solutions. J Fluid Mech 244:339–376. https://doi.org/10.1017/S0022112092003100

Bayat P, Rezai P (2017) Semi-empirical estimation of dean flow velocity in curved microchannels. Sci Rep 7(1):1–13. https://doi.org/10.1038/s41598-017-13090-z

Bayat P, Rezai P (2018) Microfluidic curved-channel centrifuge for solution exchange of target microparticles and their simultaneous separation from bacteria. Soft Matter 14(26):5356–5363. https://doi.org/10.1039/C8SM00162F

Berger SA, Talbot L, Yao LS (1983) Flow in curved pipes. Annu Rev Fluid Mech 15(1):461–512. https://doi.org/10.1146/annurev.fl.15.010183.002333

Bhagat AAS, Kuntaegowdanahalli SS, Papautsky I (2008) Continuous particle separation in spiral microchannels using dean flows and differential migration. Lab Chip 8(11):1906–1914. https://doi.org/10.1039/b807107a

Bienvenue A, Jiménez-Flores R, Singh H (2003) Rheological properties of concentrated skim milk: importance of soluble minerals in the changes in viscosity during storage. J Dairy Sci 86(12):3813–3821. https://doi.org/10.3168/jds.S0022-0302(03)73988-5

Boersma WH, Stein HN (1990) Shear thickening (dilatancy) in concentrated dispersions. AIChE J 36(3):321–332

Charjouei Moghadam M (2021) Investigation of microparticles behavior in Newtonian, viscoelastic, and shear-thickening flows in straight microfluidic channels. York University. http://hdl.handle.net/10315/39136

Chen X et al (2021) Characterization of particle movement and high-resolution separation of microalgal cells via induced-charge electroosmotic advective spiral flow. Anal Chem 93(3):1667–1676. https://doi.org/10.1021/acs.analchem.0c04251

Chung AJ (2019) A minireview on inertial microfluidics fundamentals: inertial particle focusing and secondary flow. BioChip J 13:53–63. https://doi.org/10.1007/s13206-019-3110-1

D'Avino G, Greco F, Maffettone PL (2017) Particle migration due to viscoelasticity of the suspending liquid and its relevance in microfluidic devices. Annu Rev Fluid Mech 49(1):341–360. https://doi.org/10.1146/annurev-fluid-010816-060150

Del Giudice F et al (2013) Particle alignment in a viscoelastic liquid flowing in a square-shaped microchannel. Lab Chip 13(21):4263–4271. https://doi.org/10.1039/c3lc50679g

Di Carlo D (2009) Inertial microfluidics. Lab Chip 9(21):3038–3046. https://doi.org/10.1039/b912547g

Ducloué L et al (2019) Secondary flows of viscoelastic fluids in serpentine microchannels. Microfluid Nanofluid 23(3):1–10. https://doi.org/10.1007/s10404-019-2195-0

Erdem K et al (2020) Differential sorting of microparticles using spiral microchannels with elliptic configurations. Micromachines 11(4):412. https://doi.org/10.3390/MI11040412

Fan L et al (2020) Enhanced viscoelastic focusing of particle in microchannel. Electrophoresis 41(10–11):973–982. https://doi.org/10.1002/elps.201900397

Faridi MA et al (2017) Elasto-inertial microfluidics for bacteria separation from whole blood for sepsis diagnostics. J Nanobiotechnol 15(1):1–9. https://doi.org/10.1186/s12951-016-0235-4

Feng H et al (2022) Viscoelastic particle focusing and separation in a spiral channel. Micromachines 13(3):361. https://doi.org/10.3390/mi13030361

Gossett DR et al (2012) Inertial manipulation and transfer of microparticles across laminar fluid streams. Small 8(17):2757–2764. https://doi.org/10.1002/smll.201200588

Gürgen S, Kuşhan MC, Li W (2017) Shear thickening fluids in protective applications: a review. Prog Polym Sci 75:48–72. https://doi.org/10.1016/j.progpolymsci.2017.07.003

Hasanzadeh M et al (2014) The role of shear-thickening fluids (STFs) in ballistic and stab-resistance improvement of flexible armor. J Mater Eng Perform 23(April):1182–1196. https://doi.org/10.1007/s11665-014-0870-6

Hawkes JJ et al (2004) Continuous cell washing and mixing drvien by an ultrasound standing wave within a microfluidic channel. Lab Chip 4:446–452. https://doi.org/10.1039/B408045A\n10.1039/b408045a

Huang D et al (2020) Inertial microfluidics: recent advances. Electrophoresis 41(24):2166–2187. https://doi.org/10.1002/elps.202000134

Hur SC et al (2012) Label-free enrichment of adrenal cortical progenitor cells using inertial microfluidics. PLoS ONE 7(10):e46550. https://doi.org/10.1371/journal.pone.0046550

Jiang Y, Zou S, Cao X (2016) Rapid and ultra-sensitive detection of foodborne pathogens by using miniaturized microfluidic devices: a review. Anal Methods 8(37):6668–6681. https://doi.org/10.1039/c6ay01512c

Kim B et al (2021) Viscoelastic particle focusing in human biofluids. Electrophoresis 42(21–22):2238–2245. https://doi.org/10.1002/elps.202000280

Kumar T, Ramachandraiah H, Iyengar SN (2021) High throughput viscoelastic particle focusing and separation in spiral microchannels. Sci Rep 11(1):1–13. https://doi.org/10.1038/s41598-021-88047-4

Kuntaegowdanahalli SS et al (2009) Inertial microfluidics for continuous particle separation in spiral microchannels. Lab Chip 9(20):2973–2980. https://doi.org/10.1039/b908271a

Laurell T et al (2007) Chip integrated strategies for acoustic separation and manipulation of cells and particles resulted in several national. Chem Soc Rev. https://doi.org/10.1039/b601326k

Lee YS, Wagner NJ (2003) Dynamic properties of shear thickening colloidal suspensions. Rheol Acta 42:199–208. https://doi.org/10.1007/s00397-002-0290-7

Lee YS, Wagner NJ (2006) Rheological properties and small-angle neutron scattering of a shear thickening, nanoparticle dispersion at high shear rates. Ind Eng Chem Res 45(21):7015–7024

Lee DJ et al (2013) Multiplex particle focusing via hydrodynamic force in viscoelastic fluids. Sci Rep 3:3–10. https://doi.org/10.1038/srep03258

Lee W et al (2015) 3D-printed micro fluidic device for the detection of pathogenic bacteria using size-based separation in helical channel with trapezoid cross-section. Sci Rep 5:1–7. https://doi.org/10.1038/srep07717

Li M et al (2014) A review of microfabrication techniques and dielectrophoretic microdevices for particle manipulation and separation. J Phys D Appl Phys 47:29. https://doi.org/10.1088/0022-3727/47/6/063001

Lim EJ et al (2014a) Inertio-elastic focusing of bioparticles in microchannels at high throughput. Nat Commun 5(May):1–9. https://doi.org/10.1038/ncomms5120

Lim H, Nam J, Shin S (2014b) Lateral migration of particles suspended in viscoelastic fluids in a microchannel flow. Microfluid Nanofluid 17(4):683–692. https://doi.org/10.1007/s10404-014-1353-7

Lu X et al (2017) Particle manipulations in non-Newtonian microfluidics: a review. J Colloid Interface Sci 500:182–201. https://doi.org/10.1016/j.jcis.2017.04.019

Mach AJ, di Carlo D (2010) Continuous scalable blood filtration device using inertial microfluidics. Biotechnol Bioeng 107(2):302–311. https://doi.org/10.1002/bit.22833

Martel JM, Toner M (2012) Inertial focusing dynamics in spiral microchannels. Phys Fluids 24(3):032001. https://doi.org/10.1063/1.3681228

Martel JM, Toner M (2013) Particle focusing in curved microfluidic channels. Sci Rep 3:1–8. https://doi.org/10.1038/srep03340

Martel JM, Toner M (2014) Inertial focusing in microfluidics. Annu Rev Biomed Eng 16(1):371–396. https://doi.org/10.1146/annurev-bioeng-121813-120704

Moldoveanu GM et al (2018) Viscosity estimation of Al2O3, SiO2 nanofluids and their hybrid: an experimental study. J Mol Liq 253:188–196. https://doi.org/10.1016/j.molliq.2018.01.061

Munson BR, Young DF, Okiishi TH, Huebsch WW (2009) Fundamentals of fluid mechanics. Wiley, Hoboken
Nakanishi H, Nagahiro SI, Mitarai N (2012) Fluid dynamics of dilatant fluids. Phys Rev E Stat Nonlinear Soft Matter Phys. https://doi.org/10.1103/PhysRevE.85.011401
Narayana Iyengar S et al (2021) High resolution and rapid separation of bacteria from blood using elasto-inertial microfluidics. Electrophoresis 42(23):2538–2551. https://doi.org/10.1002/elps.202100140
Nikdoost A, Rezai P (2020) Dean flow velocity of viscoelastic fluids in curved microchannels. AIP Adv 10(8):085015. https://doi.org/10.1063/5.0019021
Nikdoost A, Rezai P (2022a) Dean flow velocity of shear thickening SiO2 nanofluids in curved microchannels. Phys Fluids 34(May):062009. https://doi.org/10.1063/5.0094688
Nikdoost A, Rezai P (2022b) Microparticle manipulation in viscoelastic flows inside curvilinear microchannels: a thorough fundamental study with application to simultaneous particle sorting and washing. New J Chem 47:1635–1648. https://doi.org/10.1039/d2nj05328d
Nikdoost A et al (2021) Integration of microfluidic sample preparation with PCR detection to investigate the effects of simultaneous DNA-inhibitor separation and DNA solution exchange. Anal Chim Acta 1160:338449. https://doi.org/10.1016/j.aca.2021.338449
Nivedita N, Papautsky I (2013) Continuous separation of blood cells in spiral microfluidic devices. Biomicrofluidics 7(5):054101. https://doi.org/10.1063/1.4819275
Nivedita N, Ligrani P, Papautsky I (2017) Dean flow dynamics in low-aspect ratio spiral microchannels. Sci Rep 7(March):1–10. https://doi.org/10.1038/srep44072
Norouzi M et al (2010) Flow of second-order fluid in a curved duct with square cross-section. J Nonnewton Fluid Mech 165(7–8):323–339. https://doi.org/10.1016/j.jnnfm.2010.01.007
Nussbaum-Krammer CI et al (2015) 'Investigating the spreading and toxicity of prion-like proteins using the metazoan model organism *C. elegans*. J vis Exp 95:1–15. https://doi.org/10.3791/52321
Ookawara S et al (2004) Feasibility study on concentration of slurry and classification of contained particles by microchannel. Chem Eng J 101(1–3):171–178. https://doi.org/10.1016/j.cej.2003.11.008
Peyman SA, Iles A, Pamme N (2009) Mobile magnetic particles as solid-supports for rapid surface-based bioanalysis in continuous flow. Lab Chip 9(21):3110–3117. https://doi.org/10.1039/b904724g
Rafeie M et al (2016) Multiplexing slanted spiral microchannels for ultra-fast blood plasma separation. Lab Chip 16(15):2791–2802. https://doi.org/10.1039/c6lc00713a
Raoufi MA et al (2021) Effects of sample rheology on the equilibrium position of particles and cells within a spiral microfluidic channel. Microfluid Nanofluid 25(9):1–13. https://doi.org/10.1007/s10404-021-02475-2
Schneider CA, Rasband WS, Eliceiri KW (2012) NIH Image to ImageJ: 25 years of image analysis. Nat Methods 9(7):671–675. https://doi.org/10.1038/nmeth.2089
Segré G, Silberberg A (1961) Radial particle displacements in poiseuille flow of suspensions. Nature 189(4760):209–210. https://doi.org/10.1038/189209a0
Sivaramakrishnan M et al (2020) Active microfluidic systems for cell sorting and separation. Curr Opin Biomed Eng 13:60–68. https://doi.org/10.1016/j.cobme.2019.09.014
Sprenger L et al (2015) Simulation and experimental determination of the online separation of blood components with the help of microfluidic cascading spirals. Biomicrofluidics 9(4):044110. https://doi.org/10.1063/1.4927649
Tian F et al (2018) Label-free isolation of rare tumor cells from untreated whole blood by interfacial viscoelastic microfluidics. Lab Chip 18(22):3436–3445. https://doi.org/10.1039/c8lc00700d
Tornay R et al (2008) Dielectrophoresis-based particle exchanger for the manipulation and surface functionalization of particles. Lab Chip 8(2):267–273. https://doi.org/10.1039/b713776a
Tsai SSH et al (2011) Conformal coating of particles in microchannels by magnetic forcing. Appl Phys Lett 99(15):1–4. https://doi.org/10.1063/1.3652772
Vamerzani BZ, Norouzi M, Firoozabadi B (2014) Analytical solution for creeping motion of a viscoelastic drop falling through a Newtonian fluid. Korea Aust Rheol J 26(1):91–104. https://doi.org/10.1007/s13367-014-0010-8
Vojtíšek M, Iles A, Pamme N (2010) Rapid, multistep on-chip DNA hybridisation in continuous flow on magnetic particles. Biosens Bioelectron 25(9):2172–2176. https://doi.org/10.1016/j.bios.2010.01.034
Wagner NJ et al (2009) Shear thickening in colloidal dispersions. Phys Today 69(10):27–32. https://doi.org/10.1063/1.3248476
Xia YN, Whitesides GM (1998) Soft lithography. Annu Rev Mater Sci 37(5):551–575. https://doi.org/10.1146/annurev.matsci.28.1.153
Xiang N et al (2016) Fundamentals of elasto-inertial particle focusing in curved microfluidic channels. Lab Chip 16(14):2626–2635. https://doi.org/10.1039/c6lc00376a
Yan Z et al (2022) From Newtonian to non-Newtonian fluid: insight into the impact of rheological characteristics on mineral deposition in urine collection and transportation. Sci Total Environ 823:153532. https://doi.org/10.1016/j.scitotenv.2022.153532
Yang SH et al (2017) Multiple-line particle focusing under viscoelastic flow in a microfluidic device. Anal Chem 89(6):3639–3647. https://doi.org/10.1021/acs.analchem.6b05052
Yang SH et al (2019) Double-line particle focusing induced by negative normal stress difference in a microfluidic channel. Microfluid Nanofluid 23(2):1–10. https://doi.org/10.1007/s10404-018-2179-5
Yoon K, Jung HW, Chun M-S (2020a) Determination of velocity profiles of Bird-Carreau fluids in curvilinear microchannels using random sample consensus. Korea-Aust Rheol J 32(May):159–164. https://doi.org/10.1007/s13367-020-0015-4
Yoon K, Jung HW, Chun M-S (2020b) Secondary Dean flow characteristics of inelastic Bird-Carreau fluids in curved microchannels. Korea Aust Rheol J 32(1):61–70. https://doi.org/10.1007/s13367-020-0007-4
Yuan D et al (2018) Recent progress of particle migration in viscoelastic fluids. Lab Chip 18(4):551–567. https://doi.org/10.1039/c7lc01076a
Yuan D et al (2019) Dean-flow-coupled elasto-inertial particle and cell focusing in symmetric serpentine microchannels. Microfluid Nanofluid 23(3):1–9. https://doi.org/10.1007/s10404-019-2204-3
Zhang J et al (2016) Fundamentals and applications of inertial microfluidics: a review. Lab Chip 16(1):10–34. https://doi.org/10.1039/c5lc01159k
Zhou J, Papautsky I (2013) Fundamentals of inertial focusing in microchannels. Lab Chip 13(6):1121–1132. https://doi.org/10.1039/c2lc41248a
Zhou J, Papautsky I (2020) Viscoelastic microfluidics: progress and challenges. Microsyst Nanoeng 6(1):113. https://doi.org/10.1038/s41378-020-00218-x
Zhou Y, Ma Z, Ai Y (2020) Dynamically tunable elasto-inertial particle focusing and sorting in microfluidics. Lab Chip 20(3):568–581. https://doi.org/10.1039/c9lc01071h